

# CHANNEL ESTIMATION AND DETECTION FOR OFDM MASSIVE-MIMO IN FLAT AND FREQUENCY-SELECTIVE FADING CHANNELS<sup>1</sup>

Abdelhamid Riadi<sup>1</sup>, Mohamed Boulouird<sup>2</sup> and Moha M'Rabet Hassani<sup>1</sup>

(Received: 2-May-2020, Revised: 2-Jul.-2020 and 2-Aug.-2020, Accepted: 28-Aug.-2020)

## ABSTRACT

*In this paper, the least-squares channel estimation (LSCE) is investigated for Massive-Multiple-Input Multiple-Output (Ma-MIMO) OFDM systems based on pilot tones. The uplink (UL) transmission is considered, in which a channel estimation approach is proposed by forming a matrix equation with all the unknown channel parameters (UCPs) in one vector and estimating that vector by the least-square (LS). The mean square error (MSE) of the LSCE is computed. Flat fading and frequency-selective fading are evaluated for single and multiple OFDM symbols, concerning this MSE. The requirement of the pilot sequence is investigated in flat fading and frequency-selective fading. Besides, it is shown that the number of pilots exhibits desirable trade-offs between the base station (BS) antenna and channel taps. Rayleigh and Rician channel fading is considered to evaluate the system performance with different channel taps. Performances are compared in terms of Bit Error Rate (BER). Moreover, to enhance linear detector performance, nonlinear detectors are used. The requirement of pilot sequence and the increased receive diversity provide a lower BER for the nonlinear detector.*

## KEYWORDS

*Massive MIMO, OFDM, Flat and frequency selective fading, OSIC, Rician channel, Rayleigh channel.*

## 1. INTRODUCTION

Wireless mobile networks are classified into three broad categories. The first is satellite technologies (DVB-S2, TS2...), the second is wireless technologies (PAN, WLAN, WMAN, Wimax, ...) and the third is cellular technologies (GSM, GPRS, UMTS, LTE, 5G, ...). 5G is a promising technology based on Ma-MIMO between transceiver. Recently, in a world of great mobility, the speed and capacity of communication systems are essential elements to keep people from all over the world in communication. Ma-MIMO is also known as very large MIMO, ARGOS, large-scale antenna systems, full-dimension MIMO and hyper MIMO [1]. It's a promising emerging communication technology for 5G cellular networks [2]. Increasing the number of antennas at the BS, Ma-MIMO combined with orthogonal frequency-division multiplexing (OFDM) can support very high throughput and/or performance of the links as well as spectral efficiency [3]. In an OFDM system, like all wireless communication systems, the received signal is usually distorted by the channel characteristics. To recover the transmitted bits, the channel effect must be estimated and compensated in the receiver [4]. In fact, in a real environment, several multi-path phenomena degrade system performances. Hence, these phenomena include both small-scale fading and large-scale fading [1], [3], [5] and [6]. Channel estimation is a technique referred to in order to know channel properties. It is a very important technique in multi-cell multi-user Ma-MIMO systems. A better improvement of spectral and energy efficiency is achieved using time division duplex with pilot contamination in Rayleigh fading channels [7], while the LSCE technique is widely used for channel estimation. In addition to that, precoding at the transmitter side has a greater effect to facilitate the use of the linear detector and can help decrease complexity at the receiver [8].

On the other hand, the analytical BER performance for BPSK has been discussed for the Zero-Forcing (ZF) detector. It's associated with the Successive Interference Cancellation (SIC) for an arbitrary

<sup>1</sup> This paper is an extended version of a conference paper [27] "ZF/MMSE and OSIC Detectors for Uplink OFDM Massive MIMO Systems," Proc. of IEEE Jordan International Joint Conference on Electrical Engineering and Information Technology (JEEIT), 2019.

- 
1. A. Riadi and M. M. Hassani are with Instrumentation, Signals and Physical Systems (I2SP), Faculty of Sciences Semlalia, Cadi Ayyad University, Marrakech, Morocco, E-mails: abdelhamid.riadi@edu.uca.ac.ma and hassani@ucam.ac.ma
  2. M. Boulouird is with National School of Applied Sciences of Marrakech (ENSA-M), Cadi Ayyad University, Marrakech, Morocco, E-mail: m.boulouird@uca.ac.ma

number of transmitting and receiving antennas [9]. Similarly, the high-order M-QAM mode with ZF-OSIC receiver is discussed in [10]. Reduced complexity for MIMO Receiver and combined with the ZF-OSIC is discussed in [11], as well as in the literature, before applying the matrix inversion. The residual interference cancellation error covariance matrix of the off-diagonal elements is ignored first and the reduced-complexity approximations of soft-output MMSE-OSIC MIMO detector are studied in [12]. In addition to that, a novel soft-output MIMO MMSE OSIC detector under channel estimation is proposed in [13]. Further, a low-complexity MMSE-OSIC detector called MMSE-OBEP (Ordering Based on Error Probability) to decrease the BER of MMSE-OSIC detectors is evaluated in [14].

The performance of wireless communication systems is mainly governed by the wireless channel environment. Due to the constructive and destructive interference of multiple signal paths (multi-paths), the wireless channel is rather unpredictable. In Ma-MIMO system, the channel can be estimated by using a preamble or pilot symbol known at the receiver. Then, various interpolation techniques are employed to estimate the channel response of the subcarriers between pilot tones.

In this work, our contributions are summarized as follows:

- We propose a channel estimation approach by forming a matrix equation with all the unknown channel parameters in one vector.
- This vector is estimated in UL transmission using least-square (LS) method.
- Training symbols can be used for channel estimation.
- Constraints on pilot sequences for various scenarios are derived with respect to MSE.

This paper is organized as follows. In Section 2, a system model in the UL transmission is illustrated, in which a single cell with a BS of several antennas is considered. Section 3 is devoted to the LSCE for a Ma-MIMO system, while in Section 4, the MSE of the LSCE is described. In the same way, flat fading and frequency-selective fading according to pilot sequence requirements are investigated. Section 5 presents linear detectors. In Section 6, to improve linear detector performance, OSIC detectors are applied. Section 7 presents the simulation and results. Finally, we conclude this paper in Section 8.

## 2. COMMUNICATION SCHEME

Ma-MIMO system is considered in UL transmission from  $N_t$  users with a single antenna to a single BS with  $N_r$  antennas. The system is presented in Figure 1, for a Ma-MIMO OFDM with  $K$  sub-carriers. A cyclic prefix (CP) with length  $\nu$  is inserted to form a complete OFDM symbol. The CP is considered to be larger than the largest multi-path delay [18]-[19], [27]-[30] and [33].

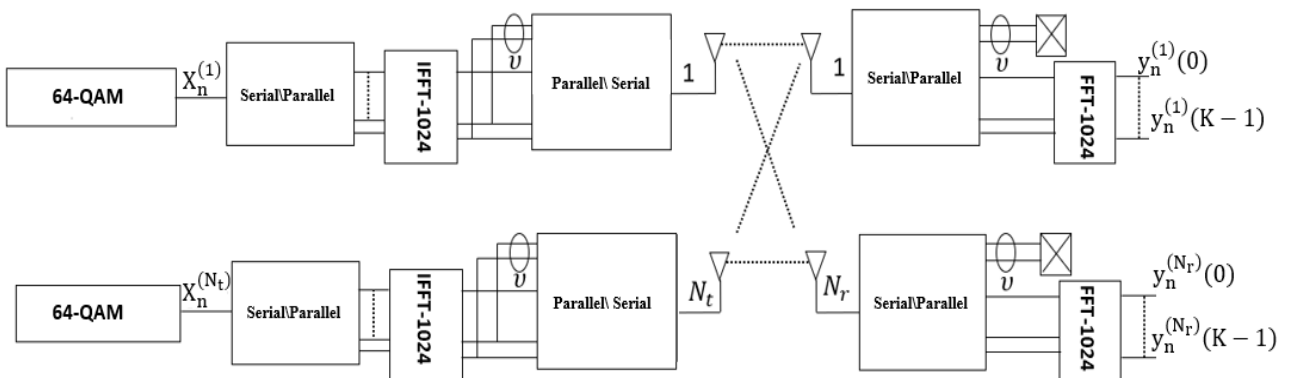


Figure 1. System model of Ma-MIMO combined with OFDM technique.

From Figure 1, the frequency response at the  $k^{th}$  subcarrier corresponding to the channel from the  $m^{th}$  transmit antenna to the  $q^{th}$  receive antenna at the  $n^{th}$  time frame (i.e., OFDM symbol) is given by [33]:

$$\begin{aligned} H_n^{(q,m)}(k) &= \sum_{l=0}^{L-1} h_n^{(q,m)}(l) e^{-j\frac{2\pi kl}{K}} \\ &= \sum_{l=0}^{L-1} h_n^{(q,m)}(l) W_K^{(k)(l)} \end{aligned} \quad (1)$$

where  $h_n^{(q,m)}(l)$  is the  $l^{th}$  channel impulse of  $h_n^{(q,m)} = [h_n^{(q,m)}(0), \dots, h_n^{(q,m)}(L-1)]^T$  with dimension  $(L \times 1)$  [35], which is the channel impulse response from the  $m^{th}$  transmit antenna to the  $q^{th}$  receive antenna, when the  $n^{th}$  OFDM symbol is transmitted. Under the assumption that  $h_n^{(q,m)}(l)$  follows the  $\mathcal{CN}(0, \sigma^2)$  [30], it can be represented by Rayleigh or Rician distribution depending on the topography of the environment.

## 2.1 Rayleigh and Rician Channel Fading

Rayleigh and Rician models are two channel models widely used in wireless communications. The Rician channel assumes that the transmission paths from the transmitter to the receiver are comprised of the dominant line of sight (LoS) path and other scattering paths. However, the Rayleigh channel consists of scattering channels from the transmitter to the receiver [17].

From Equation (1), the fading process  $h_n^{(q,m)}(l) = |h_n^{(q,m)}(l)|e^{-j\phi_n(l)}$  is assumed to be a zero-mean complex Gaussian process [36], with uniformly distributed phase  $\phi_n(l)$  on  $[0, 2\pi]$  and with Rayleigh distributed envelope  $|h_n^{(q,m)}(l)|$ ; whereas the magnitude  $|h_n^{(q,m)}(l)|$  of the  $l^{th}$  tap is a Rayleigh random variable with the probability density function (pdf) [17] and [34]:

$$pdf(x) = \frac{x}{\sigma^2} e^{-\frac{x^2}{2\sigma^2}}, \quad x \geq 0 \quad (2)$$

and the squared magnitude  $|h_n^{(q,m)}(l)|^2$  is exponentially distributed with density:

$$\frac{x}{\sigma^2} e^{-\frac{x}{\sigma^2}}, \quad x \geq 0 \quad (3)$$

This model, which is called Rayleigh fading, is quite reasonable for scattering mechanisms, where there are many small reflectors, but it is adopted primarily for its simplicity in typical cellular situations with a relatively small number of reflectors. The word Rayleigh is almost universally used for this model, but the assumption is that the tap gains are circularly symmetric complex Gaussian random variables [17].

There is a frequently used alternative model, in which the LoS path (often called a specular path) is large and has a known magnitude and there are also a large number of independent paths. In this case,  $h_n^{(q,m)}(l)$ , at least for one value of  $l$ , can be modeled as [17]:

$$h_n^{(q,m)}(l) = \sqrt{\frac{K}{K+1}} \sigma e^{j\theta} + \sqrt{\frac{1}{K+1}} \mathcal{CN}(0, \sigma^2) \quad (4)$$

with the first term corresponding to the specular path arriving with uniform phase  $\theta$  and the second term corresponding to the aggregation of the large number of reflected and scattered paths, independent of  $\theta$ . The parameter  $K$  (so-called K-factor) is the ratio of the energy in the specular path to the energy in the scattered paths; the larger  $K$  is, the more deterministic is the channel. The magnitude of such a random variable is said to have a Rician distribution. Its pdf is defined by [17]:

$$pdf(x) = \frac{x}{\sigma^2} e^{-\frac{x^2+c^2}{2\sigma^2}} I_0\left(\frac{xc}{\sigma^2}\right) \quad (5)$$

where  $c$  represents the LoS component and  $I_0(\cdot)$  is the modified zero-order Bessel function of the first kind. From Equation (5), the Rician factor is defined as  $= \frac{c^2}{2\sigma^2}$ . Moreover, where  $K = 0$ , that is to say no line of sight (NLoS) environment, Equation (5) reduces to Equation (2) of Rayleigh pdf [17]; whereas, in the next, the  $q^{th}$  receive antenna is considered at  $n^{th}$  time frame.

Based on Figure (1) and Equation (1), Ma-MIMO model is defined in the second subsection.

## 2.2 Massive MIMO Model

After removing the CP at the  $q^{th}$  receive antenna (Figure 1) and using Equation (1), the received signal  $y_n^{(q)}(k)$  can be written as [19], [27]-[30]:

$$y_n^{(q)}(k) = \sum_{m=1}^{N_t} H_n^{(q,m)}(k) x_n^{(m)}(k) + z_n^{(q)}(k) \quad (6)$$

where  $q = \{1, \dots, N_r\}$ ,  $k = \{0, \dots, K-1\}$  and  $n \in \{0, \dots, g-1\}$ . As is clear from Equation (6) and a K-subcarrier OFDM, the received signal can be rewritten as:

$$Y_n^{(q)} = \sum_{m=1}^{N_t} X_n^{(m)} G_n^{(m)} + Z_n^{(q)} \quad (7)$$

where  $Y_n^{(q)} = [y_n^{(q)}(0), y_n^{(q)}(1), \dots, y_n^{(q)}(K-1)]^T$ ,  $Z_n^{(q)} = [z_n^{(q)}(0), z_n^{(q)}(1), \dots, z_n^{(q)}(K-1)]^T$ .

Furthermore, The OFDM symbol that is transmitted from the  $m^{th}$  antenna at  $n^{th}$  time frame is defined by:

$$X_n^{(m)} = \begin{bmatrix} x_n^{(m)}(0) & 0 & 0 \\ 0 & \ddots & 0 \\ 0 & 0 & x_n^{(m)}(K-1) \end{bmatrix}_{K \times K}$$

where the  $k^{th}$  diagonal element of  $X_n^{(m)}$  is  $x_n^{(m)}(k)$ . In addition to that,  $G_n^{(m)}$  is a vector equal to  $Fh_n^{(q,m)}$  of dimension  $(K \times 1)$ . From Equation (1), we can define:

$$G_n^{(m)} = \begin{bmatrix} 1 & 1 & \dots & 1 \\ 1 & W_K^1 & \dots & W_K^{(L-1)} \\ \vdots & \vdots & \ddots & \vdots \\ 1 & W_K^{(K-1)} & \dots & W_K^{(K-1)(L-1)} \end{bmatrix}_{K \times L} h_n^{(q,m)} = F \begin{bmatrix} h_n^{(q,m)}(0) \\ \vdots \\ h_n^{(q,m)}(L-1) \end{bmatrix}_{L \times 1} \quad (8)$$

Inserting Equation (8) into Equation (7), the following expression of the received signal is obtained:

$$Y_n^{(q)} = \sum_{m=1}^{N_t} X_n^{(m)} Fh_n^{(q,m)} + Z_n^{(q)} \quad (9)$$

where  $Z_n^{(q)}$  is an AWGN with zero mean and variance of  $\sigma_n^2$ . Based on Equation (9), the LSCE will be derived in the next section.

### 3. LEAST SQUARE CHANNEL ESTIMATION

In this section, given is a K-subcarrier OFDM with a superimposed pilot sequence  $B_n^{(m)}$  and data sequence  $D_n^{(m)}$ . Let us denote  $X_n^{(m)} = D_n^{(m)} + B_n^{(m)}$ . Thus, Equation (9) can be obtained such as [27]-[30]:

$$\begin{aligned} Y_n^{(q)} &= \sum_{m=1}^{N_t} X_n^{(m)} Fh_n^{(q,m)} + Z_n^{(q)} \\ &= \sum_{m=1}^{N_t} (B_n^{(m)} + D_n^{(m)}) Fh_n^{(q,m)} + Z_n^{(q)} \\ &= \mathcal{A}_n \mathfrak{h}_n^{(q)} + \mathcal{T}_n \mathfrak{h}_n^{(q)} + Z^{(q)}(n) \end{aligned} \quad (10)$$

where  $\mathcal{A}_n = [B_n^{(1)}F, \dots, B_n^{(N_t)}F]$  of dimension  $(K \times LN_t)$ ,  $\mathcal{T}_n = [D_n^{(1)}F, \dots, D_n^{(N_t)}F]$  of dimension  $(K \times LN_t)$ . Similarly,  $B_n^{(m)}$  and  $D_n^{(m)}$  are a  $(K \times K)$  diagonal matrix defined as:

$$B_n^{(m)} = \begin{bmatrix} b_n^{(m)}(0) & 0 & 0 \\ 0 & \ddots & 0 \\ 0 & 0 & b_n^{(m)}(K-1) \end{bmatrix}_{K \times K} \quad \text{and} \quad D_n^{(m)} = \begin{bmatrix} d_n^{(m)}(0) & 0 & 0 \\ 0 & \ddots & 0 \\ 0 & 0 & d_n^{(m)}(K-1) \end{bmatrix}_{K \times K} \quad (11)$$

where  $b_n^{(m)}(k)$  and  $d_n^{(m)}(k)$  are the  $k^{th}$  diagonal element of  $B_n^{(m)}$  and  $D_n^{(m)}$ , respectively. Furthermore, the channel vector from all  $N_t$  users to  $q^{th}$  receive antenna can be noted as:

$$\mathfrak{h}_n^{(q)} = [h_n^{(q,1)H}, \dots, h_n^{(q,N_t)H}]^H \quad (12)$$

where Equation (12) is unknown channel of dimension  $(LN_t \times 1)$ . After forming a matrix equation with all the UCPs in one vector, the LSCE technique is applied to estimate this vector [1], [8] and [27]-[30]. Hence, the multiple channels can be estimated by:

$$\hat{h}_n^{(q)} = \mathcal{A}_n^+ Y_n^{(q)} \tag{13}$$

where  $\mathcal{A}_n^+ = (\mathcal{A}_n^H \mathcal{A}_n)^{-1} \mathcal{A}_n^H$  is the pseudo-inverse with a full column rank of  $LN_t$  (i.e.,  $rank(\mathcal{A}_n) = \min(gK, LN_t)$ ). Otherwise, the LS method is widely used. Low-complexity and no priori statistical knowledge about the channel and the noise are required [1], [8], [17]-[19] and [30]. Hence, using Equation (10), the estimated channels can be written as:

$$\hat{h}_n^{(q)} = h_n^{(q)} + \mathcal{A}_n^+ \mathcal{T}_n h_n^{(q)} + \mathcal{A}_n^+ Z_n^{(q)} \tag{14}$$

Further, to suppress the interference due to the data, the following condition is imposed [30]:

$$\mathcal{A}_n^+ \mathcal{T}_n = 0_{LN_t \times LN_t} \tag{15}$$

This condition is valid when  $B_n^{(m)H} D_n^{(s)} = 0_{k \times K}, \forall m, s \in \{1, \dots, N_t\}$  and  $\forall n \in \{0, \dots, g-1\}$ . Furthermore, to satisfy this condition, disjoint sets of pilot tones are chosen for training and data in each OFDM symbol, (i.e., zeros in  $B_n^{(m)}$ , where  $D_n^{(m)}$  contains non-zeros and inversely) [30]. In addition to that, let us assume  $P/g$  pilot per OFDM symbol. Thus, the dimension of  $\mathcal{A}_n^+$  becomes  $(P \times LN_t)$  and the diagonal matrix  $B_n^{(m)}$  of dimension  $(P/g \times P/g)$  is at the  $n^{th}$  time frame. Consequently, we can write Equation (14) as:

$$\hat{h}_n^{(q)} = h_n^{(q)} + \mathcal{A}_n^+ Z_n^{(q)} \tag{16}$$

Equation (16) indicates that  $\hat{h}_n^{(q)}$  is a combination of the true channel vector  $h_n^{(q)}$  plus a term affected only by the noise in the system. For zero-mean noise,  $E\{\hat{h}_n^{(q)}\} = h_n^{(q)} + \mathcal{A}_n^+ E\{Z_n^{(q)}\} = h_n^{(q)}$ ; i.e.,  $\hat{h}_n^{(q)}$  forms an unbiased estimate of  $h_n^{(q)}$ . Furthermore, the estimated channel matrix  $\hat{\mathbb{H}}_n \in \mathbb{C}^{N_r \times N_t}$ , including all users antennas  $N_t$  and all BS antennas  $N_r$ , is given by [30]:

$$\hat{\mathbb{H}}_n = \begin{bmatrix} \hat{h}_n^{(1,1)} & \dots & \hat{h}_n^{(1,N_t)} \\ \vdots & & \vdots \\ \hat{h}_n^{(q,1)} & \dots & \hat{h}_n^{(q,N_t)} \\ \vdots & & \vdots \\ \hat{h}_n^{(N_r,1)} & \dots & \hat{h}_n^{(N_r,N_t)} \end{bmatrix} = \begin{bmatrix} \hat{h}_n^{(1)T} \\ \vdots \\ \hat{h}_n^{(N_r)T} \end{bmatrix} = [\hat{\mathcal{H}}_n^{(1)}, \dots, \hat{\mathcal{H}}_n^{(N_t)}] \tag{17}$$

where the estimated channel vector at the  $n^{th}$  time frame and user position  $i$  is given by  $\hat{\mathcal{H}}_n^i = [\hat{h}_n^{(1,i)T}, \dots, \hat{h}_n^{(N_r,i)T}]^T$ ; whereas training OFDM symbols are used over the time indices  $n \in \{0, \dots, g-1\}$  [1], [8] and [27]-[30]. Thus, Equation (10) can be written as:  $Y^{(q)} = \mathcal{A} h^{(q)} + \mathcal{T} h^{(q)} + Z^{(q)}$ , where the received signal at the  $q^{th}$  receive antenna can be noted by:  $Y^{(q)} = [Y_0^{(q)T}, \dots, Y_{g-1}^{(q)T}]^T$  and the noise vector becomes  $Z^{(q)} = [Z_0^{(q)T}, \dots, Z_{g-1}^{(q)T}]^T$ . The channel vector is  $h^{(q)} = [h_0^{(q)}, \dots, h_{g-1}^{(q)}]$ . Similarly,  $\mathcal{A}$  and  $\mathcal{T}$  are noted as:

$$\mathcal{A} = \begin{bmatrix} \mathcal{A}_0 \\ \vdots \\ \mathcal{A}_{g-1} \end{bmatrix} = \begin{bmatrix} B_0^{(1)}F & \dots & B_0^{(N_t)}F \\ \vdots & & \vdots \\ B_{g-1}^{(1)}F & \dots & B_{g-1}^{(N_t)}F \end{bmatrix} \text{ and } \mathcal{T} = \begin{bmatrix} \mathcal{T}_0 \\ \vdots \\ \mathcal{T}_{g-1} \end{bmatrix} = \begin{bmatrix} D_0^{(1)}F & \dots & D_0^{(N_t)}F \\ \vdots & & \vdots \\ D_{g-1}^{(1)}F & \dots & D_{g-1}^{(N_t)}F \end{bmatrix}$$

respectively. The same process of channel estimation has been carried out for all  $n$  as the  $n^{th}$  time frame. Moreover, after channel estimation at the  $q^{th}$  receive antenna and  $n^{th}$  time frame (i.e., Equation 13), the MSE is derived in the next section.

#### 4. MEAN SQUARE ERROR OF LS ESTIMATOR

In this section, the MSE of LSCE is computed. Hence, the MSE of LSCE is given as [18], [21]:

$$\begin{aligned}
MSE_n &= \frac{1}{LN_t} E \left\{ \left\| \hat{\mathbf{h}}_n^{(q)} - \mathbf{h}_n^{(q)} \right\|^2 \right\} \\
&= \frac{1}{LN_t} E \left\{ \left\| \mathcal{A}_n^+ \mathbf{Z}_n^{(q)} \right\|^2 \right\} \\
&= \frac{1}{LN_t} \text{tr} \{ \mathcal{A}_n^+ E \left( \mathbf{Z}_n^{(q)} \mathbf{Z}_n^{(q)H} \right) \mathcal{A}_n^{+H} \}
\end{aligned} \tag{18}$$

For zero-mean white noise, we have:  $E \left( \mathbf{Z}_n^{(q)} \mathbf{Z}_n^{(q)H} \right) = \sigma_n^2$ . Then, the MSE can be written as:

$$MSE_n = \frac{\sigma_n^2}{LN_t} \text{tr} \{ (\mathcal{A}_n^H \mathcal{A}_n)^{-1} \} \tag{19}$$

Using a similar argument as in [18], [21] and [27]-[29], we can show that in order to obtain the minimum MSE of the LSCE subject to a fixed power  $\mathcal{P}$  dedicated for training, we require  $\mathcal{A}_n^H \mathcal{A}_n = \mathcal{P} I_{LN_t \times LN_t}$ . The minimum MSE is given by:

$$MSE_n^{\min} = \frac{\sigma_n^2}{\mathcal{P}} \tag{20}$$

In the next part of this paper, flat fading and frequency-selective fading are investigated with respect to this MSE.

#### 4.1 Flat Fading and Frequency-selective Fading

In this subsection, flat fading and frequency-selective fading are presented, with regard to MSE of the LSCE. At first,  $g = 1$  (i.e., one OFDM symbol) is considered and then, the study is extended to multiple OFDM symbols (i.e.,  $g > 1$ ). When  $g = 1$ , training over the time index  $n = 0$  and  $\mathcal{A}_n^H \mathcal{A}_n$  can be rewritten as [18], [21]:

$$\mathcal{A}_n^H \mathcal{A}_n = \begin{bmatrix} C_{1,1} & \dots & C_{1,N_t} \\ \vdots & \ddots & \vdots \\ C_{N_t,1} & \dots & C_{N_t,N_t} \end{bmatrix} \tag{21}$$

where  $C_{m,s}$  is a sub-matrix of  $\mathcal{A}_n^H \mathcal{A}_n$ , with dimension  $(L \times L)$ , that is given by:

$$C_{m,s} = F^H B^{(m)H} B_0^{(s)} F \tag{22}$$

As previously mentioned, in order to obtain the minimum MSE of the LSCE, it is necessary to fix the power  $\mathcal{P}$  for training. Hence,  $\mathcal{A}_n^H \mathcal{A}_n = \mathcal{P} I_{LN_t \times LN_t}$ ; that is to say [18], [21]:

$$\mathcal{A}_n^H \mathcal{A}_n = \begin{cases} \mathcal{P} I_{L \times L}, & \text{if } m = s \\ 0_{L \times L}, & \text{if } m \neq s \end{cases} \tag{23}$$

The positions of the  $P$  pilot tones used for training are defined as  $\{k_0, k_1, k_2, \dots, k_{P-1}\}$ . In addition to that,  $F$  can be noted as  $F = [f_0, f_1, f_2, \dots, f_{L-1}]$ , where  $f_l = \left[ e^{-\frac{j2\pi l k_0}{K}}, e^{-\frac{j2\pi l k_1}{K}}, e^{-\frac{j2\pi l k_2}{K}}, \dots, e^{-\frac{j2\pi l k_{P-1}}{K}} \right]^T$ . Thereby, from Equation (23), when  $m = s$ , the power on the  $i^{\text{th}}$  pilot tone of the  $m^{\text{th}}$  transmit antenna can be noted as  $p_i^m$ . Thus,  $\sum_{i=0}^{P-1} p_i^m = \mathcal{P}$  [18], [19] and [21]. Therefore, Equation (22) can be written as follows:

$$C_{m,m} = F^H \text{diag} \{ [p_0^m, p_1^m, \dots, p_{P-1}^m]^H \} F \tag{24}$$

From Equation (24), the  $(n, d)^{\text{th}}$  entry of the sub-matrix  $C_{m,m}$  is obtained as:

$$[C_{m,m}]_{n,d} = f_n^H \text{diag} \{ [p_0^m, p_1^m, \dots, p_{P-1}^m]^H \} f_d \tag{25}$$

which is equivalent to:

$$[C_{m,m}]_{n,d} = \begin{cases} \mathcal{P}, & \text{if } n = d \\ \sum_{i=0}^{P-1} p_i^m e^{-\frac{j2\pi k_i(n-d)}{K}}, & \text{if } n \neq d \end{cases} \tag{26}$$

Thereby, to satisfy the first part of Equation (23), we need:

$$\sum_{i=0}^{P-1} p_i^m e^{-\frac{2j\pi k_i \phi}{K}} = \mathcal{P} \delta(\phi), \quad \forall \phi \in \{-L+1, \dots, L-1\} \tag{27}$$

Accordingly, the above condition is satisfied if and only if the following conditions are satisfied [18], [19] and [21]:

- $p_i^m = \frac{P}{P}, \forall i \in \{0, 1, \dots, P - 1\}$  and  $\forall m \in \{1, \dots, N_t\}$
- $k_i = p_0 + pV, \forall \phi \in \{-L + 1, \dots, L - 1\} \setminus \{0\}$ , where  $V \in \mathbb{Z}$  such that  $PV\phi/K \in \mathbb{Z}$  and  $V\phi/K \notin \mathbb{Z}, \forall \phi \in \{-L + 1, \dots, L - 1\}$ , and  $p_0 \in \{0, 1, \dots, V - 1\}$  is some offset.

Table 1. Pilot sequence for various scenarios.

Configurations	Pilot sequence requirement
Flat Fading: L=1	Equipowered+ Equispaced+ Orthogonal
Frequency-selective Fading: L>1	Equipowered+ Equispaced+ Phase Shift Orthogonal $\forall \phi \in \{-L + 1, \dots, L - 1\}$

Hence, the first condition means that the pilot tone must be equipowered. Moreover, the second condition means that the pilot tones must be equispaced. For a minimum number of pilot tones or a maximum spacing, we have  $PV = K$  or  $V = K/P$ . For a practical system with inexpensive, fast and simple implementation of the FFT, the number of subcarriers must be power of 2, on the one hand. On the other hand, the P pilot tones should divide K (i.e., P must be power of 2). Hence,  $P \geq LN_t$ ; that is to say  $P = 2^{\log_2 LN_t}$  [19]. In the case where L= 1 (i.e., flat fading) pilot sequences must be equipowered, equispaced and orthogonal for various transmit antennas. When L > 1 (i.e., frequency-selective fading), the pilot sequences must be equipowered, equispaced and phase shift orthogonal for various transmit antennas (Table 1) [18], [21].

When,  $g > 1$  (i.e., multiple OFDM symbols) is considered and training over the time indices  $n \in \{0, \dots, g - 1\}$ , Equations (22) and (27) become:

$$C_{m,s} = \sum_{n=0}^{g-1} F_n^H B^{(m)H} B_n^{(s)} F_n \tag{28}$$

$$\sum_{n=0}^{g-1} \sum_{i=0}^{P-1} p_{i,n}^m e^{-\frac{2j\pi k_{i,n} \phi}{K}} = \mathcal{P} \delta(\phi), \quad \forall \phi \in \{-L + 1, \dots, L - 1\} \tag{29}$$

where the positions of the P pilot tones used for training become  $\{k_{0,n}, k_{1,n}, k_{2,n}, \dots, k_{P-1,n}\}$  and  $F_n = [f_{0,n}, f_{1,n}, f_{2,n}, \dots, f_{L-1,n}]$ , where  $f_{i,n} = \left[ e^{-\frac{j2\pi k_{0,n}}{K}}, e^{-\frac{j2\pi k_{1,n}}{K}}, e^{-\frac{j2\pi k_{2,n}}{K}}, \dots, e^{-\frac{j2\pi k_{P-1,n}}{K}} \right]^T$ . The power on the  $i^{th}$  pilot tone of the  $m^{th}$  transmit antenna can be rewritten as:  $p_{i,n}^m$ , thus  $\sum_{n=0}^{g-1} \sum_{i=0}^{P-1} p_{i,n}^m = \mathcal{P}$  [18], [19] and [21]. Furthermore, after getting the channel estimation at the BS, the requirement of the pilot sequence in flat fading and frequency-selective fading is defined. The data is detected using linear and nonlinear detectors. The detection method treats all transmitted signals as interferences, except for the desired stream from the target transmit antenna. Therefore, interference signals from other transmit antennas are minimized or nullified in the course of detecting the desired signal from the target transmit antenna, given the knowledge of the received vector and the channel matrix (i.e., Equation 17). To facilitate the detection of the desired signal from each antenna, the effect of the channel is inverted by a transformation matrix T.

### 5. LINEAR DETECTORS

In UL transmission, the data sequence is generated by linear detectors after channel estimation is carried out at the BS in order to obtain data sequences. Linear methods are used to generate data sequences of transmitted symbols through a linear transformation of the received vector y [22], [27]-[30]. These methods take the form of  $d = Ty$ , where T is a transformation matrix, as shown in Figure 2.

#### 5.1 Zero Forcing Detector

The Zero Forcing (ZF) detector is a simple linear detector, in which the linear transformation on the received vector is carried out using the pseudo-inverse of the  $\hat{H}_n$  matrix (i.e., Equation 17). The ZF detector completely cancels the interference from other signals (hence the name zero-forcing or interference-nulling detector) [2], [22]-[23] and [27]-[29]. Then, the linear transformation matrix is

given by:

$$T_{ZF} = \hat{\mathbb{H}}_n^+ \tag{30}$$

where  $\hat{\mathbb{H}}_n^+ = (\hat{\mathbb{H}}_n^H \hat{\mathbb{H}}_n)^{-1} \hat{\mathbb{H}}_n^H$  is the pseudo-inverse of dimension  $(N_t \times N_r)$ .

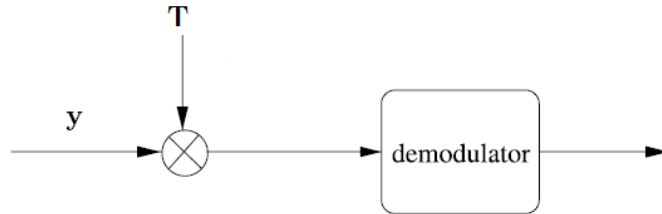


Figure 2. Conceptual illustration of linear MIMO detectors [22].

### 5.2 Minimum Mean Square Error Detector

The Minimum Mean Square Error (MMSE) detector is a linear detector, the transformation matrix of which minimizes the mean square error between the transmit vector  $X$  and the received vector  $Y$ . The transformation matrix  $T_{MMSE}$  is given by the solution to the following minimization problem [2], [22]-[23] and [27]-[29]:

$$T_{MMSE} = \arg_{T_{MMSE}} \min E(\|X - T_{MMSE}Y\|_2^2) \tag{31}$$

where  $Y = [Y_n^{(1)}, \dots, Y_n^{(N_t)}]^T$  and  $X = [X_n^{(1)}, \dots, X_n^{(N_t)}]^T$ . Finally, the transformation  $T_{MMSE}$  can be defined as:

$$T_{MMSE} = (\hat{\mathbb{H}}_n^H \hat{\mathbb{H}}_n + 2\sigma_n^2 I)^{-1} \hat{\mathbb{H}}_n^H \tag{32}$$

where  $\sigma_n^2$  is the noise power.

## 6. OSIC SIGNAL DETECTION

Detectors based on interference cancellation belong to the class of non-linear detectors, where interference due to detected stream is removed in multiple stages [22], [27] and [30]. Popular interference cancellation techniques include Ordered Successive Interference Cancellation (OSIC), which is used to improve linear detector performance without increasing the complexity significantly. OSIC is known for its simplicity. Figure 3 gives an example of three spatial streams [27], [30]. Hence, based on Equation (30), The steps involved in OSIC based detection can be summarized as follows:

1. Initially, the first stream is detected using the first row vector of Equation (30),
2. After detection and slicing to produce  $X_1$ , the remaining signal in the first stage is formed by subtracting it from the received signal as  $y_1 = y - \hat{\mathcal{H}}_n^1 X_1$ .

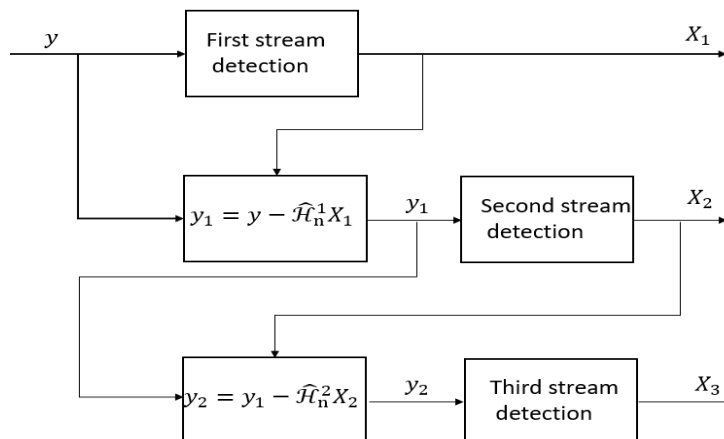


Figure 3. Illustration of OSIC signal detection example of three spatial streams (i.e.,  $N_t=3$ ) [30].

3. The interference due to the detected stream in the first stage is canceled.
4. Another stream is detected and sliced in the second stage to produce  $X_2$ .
5. Similarly, the remaining signal and the interference in the second stage are formed by subtracting it from the received signal as  $y_2 = y_1 - \hat{\mathcal{H}}_n^2 X_2$ .

Hence, the same processes of detection and slicing as well as interference cancelation are reproduced in the next stages [2], [24]-[27] and [30] due to the error propagation caused by erroneous decisions in the previous stages. The order of detection has significant influence on the overall performance of OSIC detection. In the next part of this section, two methods to reduce error propagation are described:

Firstly: SINR-based Ordering (SINR-BO). In this case, streams with a high post detection Signal-to-Interference-plus-Noise Ratio (SINR) are detected first [1], [27] and [30]. Based on the transformation matrix  $T_{MMSE}$ , the post-detector with SINR is defined as:

$$SINR_i = \frac{E_x |T_{i,MMSE} \hat{\mathcal{H}}_n^i|^2}{E_x \sum_{l \neq i} |T_{l,MMSE} \hat{\mathcal{H}}_n^l|^2 + \sigma_n^2 \|T_{i,MMSE}\|^2} \quad (33)$$

where  $T_{i,MMSE}$  is the  $i^{th}$  row of matrix (Equation 32),  $\hat{\mathcal{H}}_n^i$  is the  $i^{th}$  column vector of the estimated channel matrix  $\hat{\mathbb{H}}_n$  at  $n^{th}$  time OFDM symbol with  $i = 1, 2, \dots, N_t$ . Also,  $E_x$  is the transmitted signal energy. Furthermore, once the  $N_t$  of SINR are calculated based on Equation (32), we choose the corresponding layer with the highest SINR. In addition to that, the procedure discussed above is applied for symbol detection. Furthermore, Equation (32) is modified by the suppression of the channel gain vector equivalent to the data detected. Otherwise, the total number of SINR values to be calculated is  $\sum_{i=1}^{N_t} i = \frac{N_t(N_t+1)}{2}$  [27], [30].

Secondly: SNR-based Ordering (SNR-BO). In this method, streams with a higher Signal-to-Noise Ratio (SNR) are detected first [1], [27] and [30]. Similarly based on the transformation matrix  $T_{ZF}$ , the SNR is defined as:

$$SNR_i = \frac{E_x}{\sigma_n^2 \|T_{i,ZF}\|^2} \quad (34)$$

where  $i = 1, 2, \dots, N_t$ . Similarly, the procedure discussed in the first method can be used. In this method, the number of SNR values to be calculated is also given by  $\sum_{i=1}^{N_t} i = \frac{N_t(N_t+1)}{2}$  [1], [27] and [30].

## 7. SIMULATION RESULTS

In this section, a collection of performance results concerning two linear detectors (MMSE and ZF) as well as the nonlinear OSIC detectors is presented, in which their performances are evaluated in terms of BER. Hence, the computer simulation parameters are given, as shown in Table 2.

Table 2. Computer simulation parameters.

Parameters	Values
OFDM-Subcarriers	1024
OFDM symbol number (g)	10
M-QAM Modulation	64-QAM
Channel model	Rayleigh and Rician
L-taps	1, 6 and 10
$N_t \times N_r$	$50 \times 100$ , $50 \times 200$ and $50 \times 300$

In this part, various channel taps (i.e., 1, 6 and 10) are simulated as i.i.d. Firstly, one OFDM subcarrier (i.e., OFDM symbol) with  $K = 1024$  (Figure 4) and a CP of  $v = 256$  is considered. The number of pilot tones dedicated for training is  $P=K/2$ , which are equipowered and equispaced or equipowered, equispaced and phase shift orthogonal. The length of data sequences is equal to  $K/2$  (Figure 4). Hence,

training is performed over  $g$  consecutive OFDM symbols using Monte Carlo simulation. Throughout this simulation, the number of terminals ( $N_t$ ) is set to be 50 (i.e., respecting the condition treated in subsection 4.1; that is  $P \geq LN_t$ ).

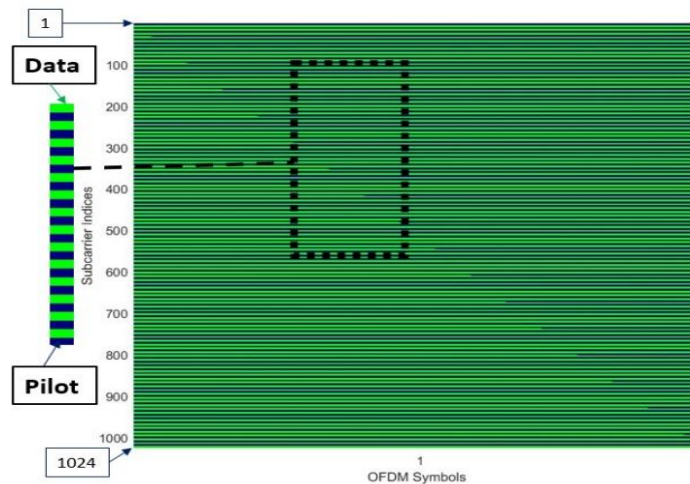


Figure 4. OFDM subcarrier for a Ma-MIMO system with  $N_t = 50$  and  $N_r = 100$  transmit and receive antennas, respectively.

In other words, Figure 5 shows the distributions for Rayleigh and Rician fading channels. It also demonstrates an example for  $K = -40$  dB. The Rician distribution approaches the Rayleigh distribution and for  $K = 15$  dB, the Rician distribution approaches the Gaussian distribution. In the remainder of this paper, we assume  $K = -40$  dB for the Rayleigh fading channel and  $K \geq 15$  dB for the Gaussian channel.

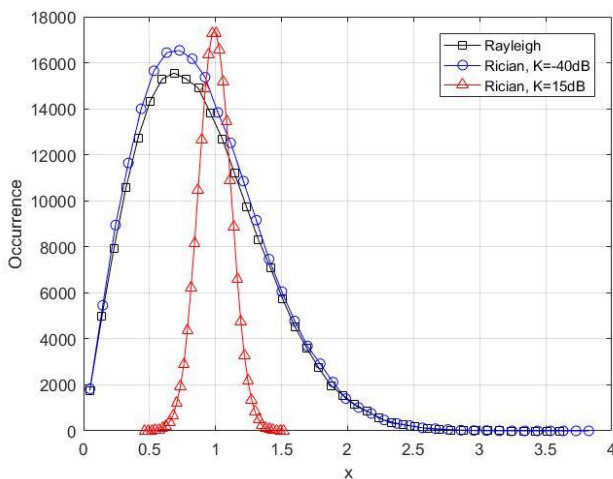


Figure 5. Distributions for Rayleigh and Rician fading channels.

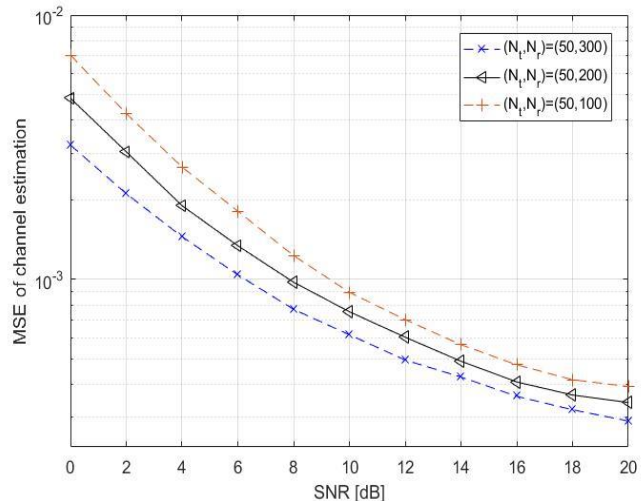


Figure 6. Channel estimation error vs. SNR for Rayleigh channel.

Figure 6 shows the channel estimation error for  $N_r = 100, 200$  and  $300$  when Rayleigh channel is applied. The channel estimation performance improves when  $N_r$  increases and SNR increases. In related work [32], for  $N_r \times N_t = 128 \times 64$  Ma-MIMO system, Generalized Approximate Message Passing Detector (GAMPD) achieves an MSE of around 0.3 at SNR = 0 dB, while at SNR=2 dB, its MSE is around 0.1 for  $N_r \times N_t = 128 \times 128$ . Moreover, for  $N_r \times N_t = 100 \times 50$  (Figure 6), our proposed method achieves an MSE of around 0.00705 at SNR = 0 dB and 0.00424 at SNR= 2 dB. In addition, when more receive antennas are used, more spatial diversity can result in a better chance to successfully detect the data.

In the simulations, Ma-MIMO with multiple receiver antennas ( $N_r=100, 200$  and  $300$ ) and 64-QAM modulation is used. Figure 7 shows a plot of BER versus SNR for  $L = 1$  (i.e., flat fading), when a Rayleigh fading channel is employed. It is clear that the BER performance of all detectors decreases

with a higher SNR. However, the MMSE performance is very close to the ZF performance. In this way, at high SNRs (i.e., small  $\sigma$ ), MMSE behaves like ZF, since the second term inside the inverse operation

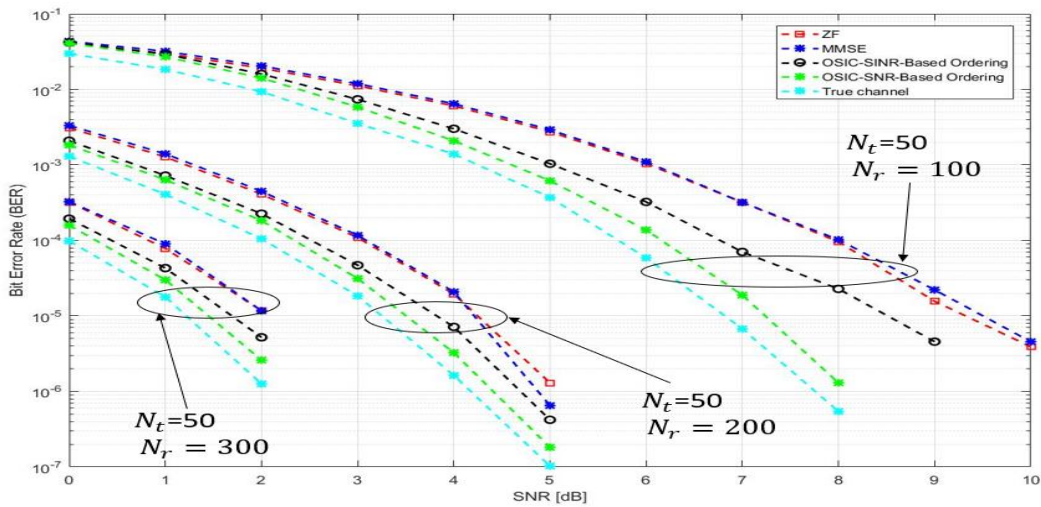


Figure 7. BER vs. SNR for  $L=1$  using ZF, MMSE and various OSIC detectors for Rayleigh channel.

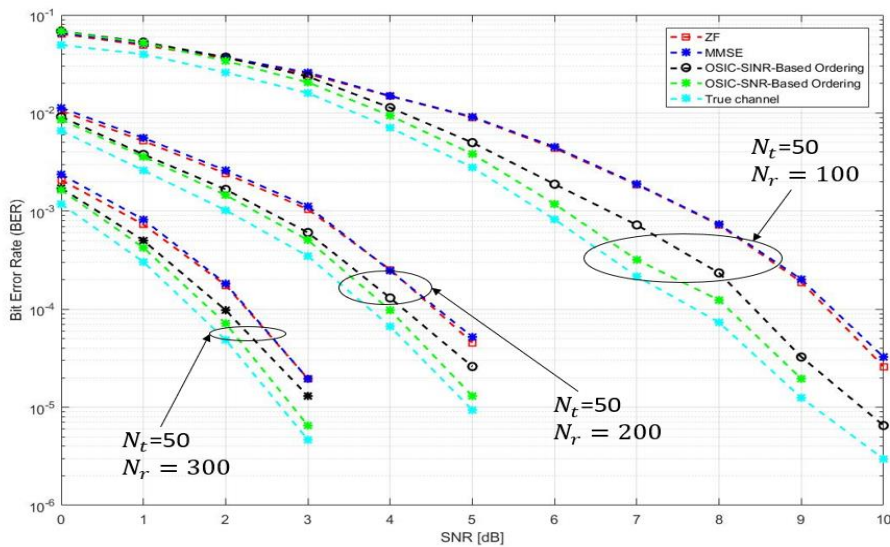


Figure 8. BER vs. SNR for  $L=6$  using ZF, MMSE and various OSIC detectors for Rayleigh channel.

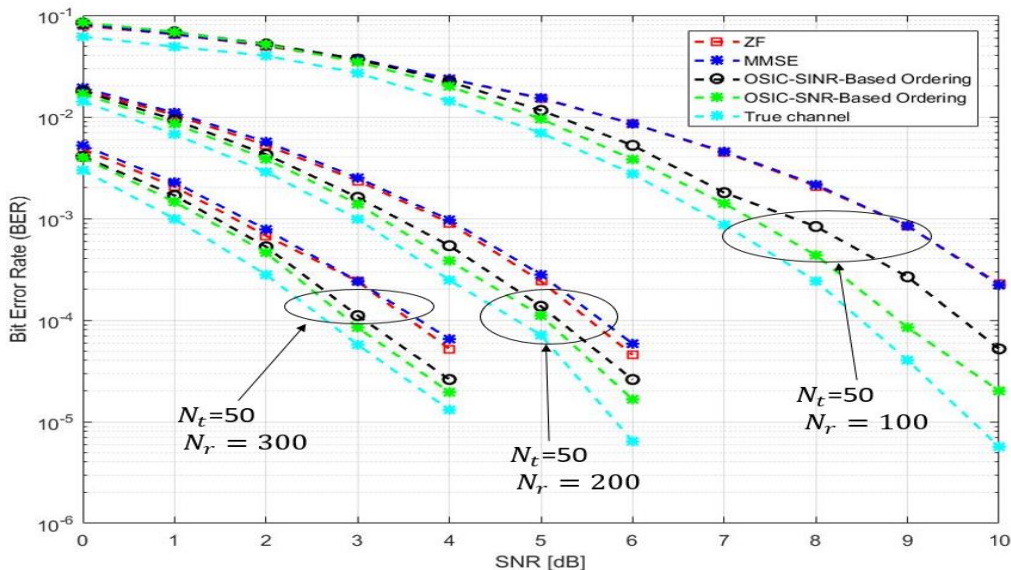


Figure 9. BER vs. SNR for  $L=10$  using ZF, MMSE and various OSIC detectors for Rayleigh channel.

in Equation (32) becomes negligible. On the other hand, the performance of the OSIC detection method with SNR-BO outperforms all other detectors and is close to true channel performance. In related work [31], for  $N_r \times N_t = 128 \times 16$  Ma-MIMO system, refinement Jacobi (RJ)-based detector achieves a BER of around  $3.2 \times 10^{-3}$  at SNR = 13 dB, while for the  $N_r \times N_t = 256 \times 16$  Ma-MIMO system, it achieves a BER of around  $5 \times 10^{-5}$  at the same SNR. For  $N_r \times N_t = 100 \times 50$  Ma-MIMO, for example, ZF detector achieves a BER of around  $319 \times 10^{-6}$  (i.e.,  $0.319 \times 10^{-3}$ ) at SNR=7 dB. In this work and in [31], the SNR gap between the ZF and RJ-based detector at  $10^{-3}$  BER is just about 6 dB.

Otherwise, Figures 8 and 9 show the BER performance comparison between linear and nonlinear detectors when the number of channel taps is  $L=6$  and  $10$ , respectively. With an increase of channel tap number the performance of all detectors is degraded. Hence, system performance is sensitive to a higher channel taps (i.e., high frequency-selective fading). In addition to that, the gap between the OSIC-SNR-BO detector and true channel performance becomes small as the number of BS antennas increases. In related work [32], for  $N_r \times N_t = 128 \times 80$  Ma-MIMO system, Generalized Approximate Message Passing Detector (GAMPD) achieves a BER of around  $10^{-2}$  at SNR = 4.3 dB. For  $N_r \times N_t = 100 \times 50$  Ma-MIMO, for example, ZF detector achieves an SNR=5.74 dB at the same BER. Thus, the SNR gap between the ZF detector and GAMPD detector is just about 1.44 dB. In addition, ZF detector achieves a better performance and surpasses the GAMPD detector with a gap of 3.315 dB at BER of  $10^{-2}$  for a Ma-MIMO of  $N_r \times N_t = 200 \times 50$ . Moreover, at  $N_r = 300$ , ZF detector is close to approximate message passing (AMP) algorithms [33], with a gap of 0.06 dB, despite a high system sensitivity to noise (i.e., 64-QAM) and high frequency-selective fading channel. The OSIC-SNR-BO detector is useful for a high multi-path fading channel or equivalently, a frequency-selective fading channel.

In addition to that, Figure 10 presents the BER in a flat Rician channel fading in the case of  $K = 15$  (i.e., LoS) and the number of antennas at the BS equal to 100. The simulation result illustrates the convergence of all detectors over a high range of SNR and provides a bad performance. Despite the presence of multi-path effects, the system took the thermal noise from the receiver as a single source of noise (i.e., Gaussian channel). In addition, the channel behaves as the simplest statistical channel from an implementation, but not necessarily the most realistic one. However, when the BS antennas increase to 300, the system performance for the same range of SNR is improved. This improvement is likely due to the potential diversity at the BS and at the ordering (selection) in OSIC. In the case of  $K = -40$  (NLoS), the BER decreases more and is close to Rayleigh performance. When the BS antennas increase to 300, the simulation result shows the best performance at a smaller range of SNR. Thereby, the OSIC-SNR-BO usually provides the best performance and is close to the true channel. In the same way, we consider the case of frequency-selective fading (i.e.,  $L = 6$  and  $10$ , Figures 11 and 12, respectively). From these figures, we can see that the BER is also sensitive to the channel taps and the Rician factor. A higher number of channel taps provides a higher BER at both  $K=15$  and  $-40$ . Similarly, when the BS antennas

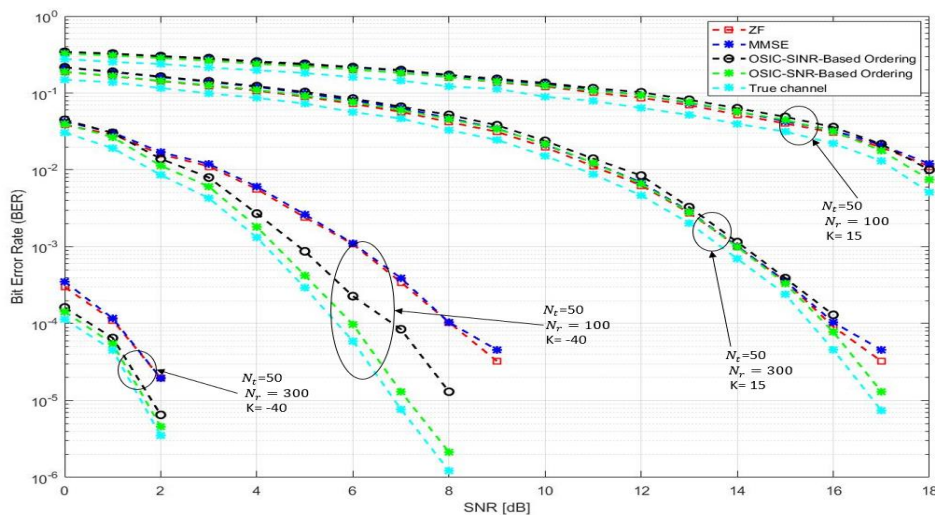


Figure 10. BER vs. SNR for  $L=1$  using ZF, MMSE and various OSIC detectors for Rician channel with  $K=-40$  and  $15$ .

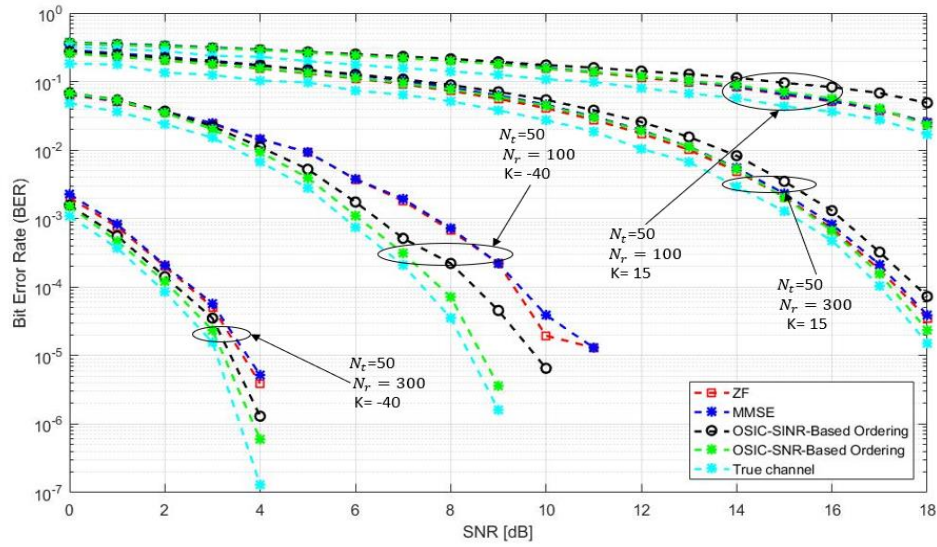


Figure 11. BER vs. SNR for  $L=6$  using ZF, MMSE and various OSIC detectors for Rician channel with  $K= -40$  and  $15$ .

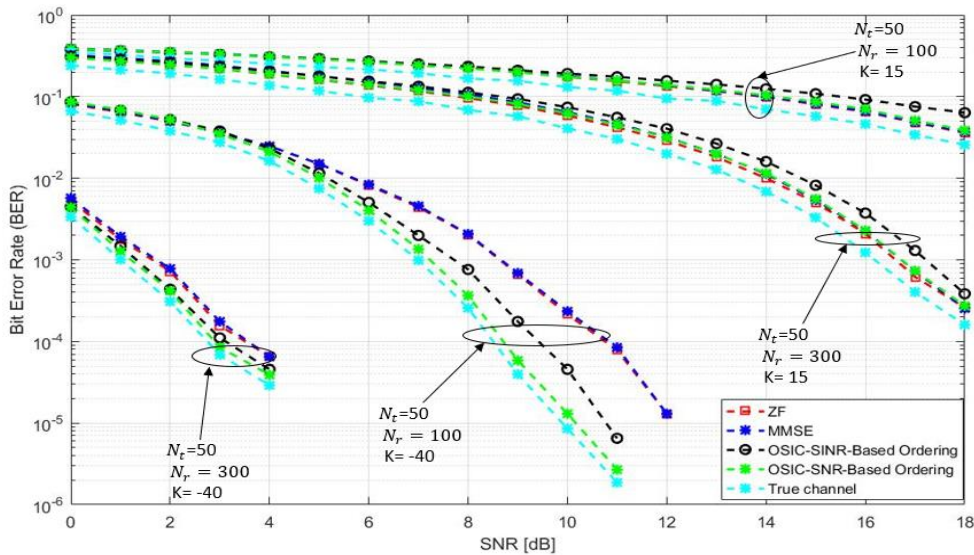


Figure 12. BER vs. SNR for  $L=10$  using ZF, MMSE and various OSIC detectors for Rician channel with  $K= -40$  and  $15$ .

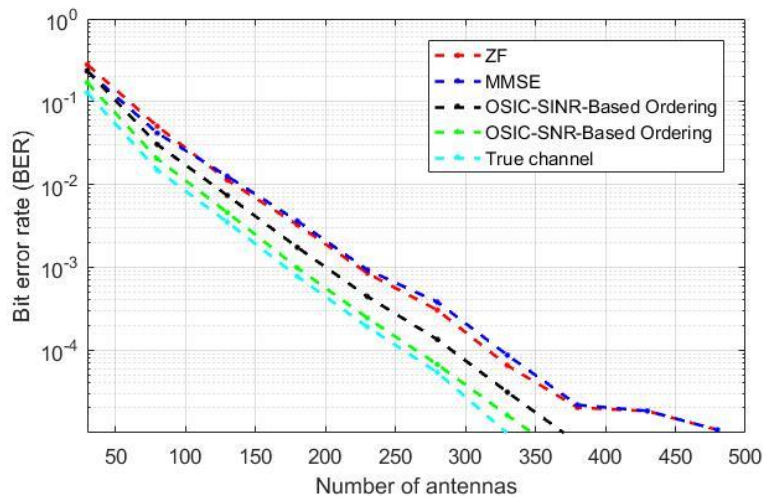


Figure 13. BER vs. number of antennas at the base station for  $L=10$  using ZF, MMSE and various OSIC detectors for Rayleigh channel.

are equal to 300, the BER decreases more. Under a lower Rician factor, the system took into account the channel fading. In addition, the antenna diversity at the reception favors a constructive signal overlay. Thus, the system performance is improved and frequency-selective fading effect is compensated. In addition to that, OSIC-SNR-BO provides a better performance which is close to true channel performance.

Furthermore, Figure 13 presents the BER performance of linear detectors and nonlinear detectors with the number of antennas at the BS. The number of channel taps is equal to 10 and the SNR is set to be with a mean value 8 dB. It is clearly shown that BER decreases over a high number of antennas. In addition to that, it is observed that MMSE detector achieves a performance which is close to the performance achieved by the ZF detector. For more than 300 antennas, OSIC-SNR-BO performs slightly better than OSIC-SINR-BO due to high interference (i.e.,  $N_t = 50$ ). More interestingly, this improved performance of OSIC-SNR-BO compared to that of OSIC-SINR-BO increases remarkably as  $N_r$  increases.

## 8. CONCLUSIONS

In this paper, we have successively evaluated the LSCE performance in UL transmission. ZF, MMSE and OSIC detectors for a Ma-MIMO system are combined with high-order modulation 64-QAM and OFDM technique. The performance of a Ma-MIMO system in Rayleigh and Rician channel fading is analyzed with channel taps and Rician factor. The presence of many fading phenomena characterized by flat fading and frequency-selective fading degrades the system performance. Joining a large number of antennas at the BS with equipowered, equispaced and phase shift orthogonal pilot sequences can achieve a very low BER. At a higher number of antennas at the BS, the OSIC-SNR-BO provides a better performance which is close to true channel performance, while the effect of frequency-selective fading is canceled in a lower signal to noise ratio.

## REFERENCES

- [1] E. G. Larsson, O. Edfors, F. Tufvesson and T. L. Marzetta, "Massive MIMO for Next Generation Wireless Systems," *IEEE Communications Magazine*, vol. 52, no. 2, pp. 186-195, 2014.
- [2] A. Chockalingam and B. Sundar Rajan, *Large MIMO Systems*, Cambridge University Press, 2014.
- [3] F. Rusek, D. Persson, B. K. Lau, E. G. Larsson, T. L. Marzetta, O. Edfors and F. Tufvesson, "Scaling up MIMO: Opportunities and Challenges with Very Large Arrays," *IEEE Signal Processing Magazine*, vol. 30, No. 1, pp. 40-60, 2013.
- [4] S. Singh et al., "Review of DFT-based Channel Estimation Techniques in OFDM over Multipath Channel," *International Journal of Recent Research Aspects*, vol. 3, no. 4, pp. 8-11, December 2016.
- [5] N. Jalden, P. Zetterberg, B. Ottersten, A. Hong and R. Thoma, "Correlation Properties of Large-scale Fading Based on Indoor Measurements," *Proc. of IEEE Wireless Communications and Networking Conference (WCNC 2007)*, pp. 1894-1899, Kowloon, China, 2007.
- [6] A. Ashikhmin, T. L. Marzetta and L. Li, "Interference Reduction in Multi-cell Massive MIMO Systems I: Large-scale Fading Precoding and Decoding," *IEEE Transactions on Information Theory*, [Online], Available: <https://arxiv.org/abs/1411.4182>, November 2014.
- [7] F. A. P. de Figueiredo, F. A. C. M. Cardoso, I. Moerman and G. Fraidenraich, "Channel Estimation for Massive MIMO TDD Systems Assuming Pilot Contamination and at Fading," *EURASIP Journal on Wireless Communications and Networking*, vol. 2018, no. 1, Article no. 14, 2018.
- [8] E. Ohlmer and G. Fettweis, "Linear and Non-linear Detection for MIMO- OFDM Systems with Linear Pprecoding and Spatial Correlation," *Proc. of IEEE Wireless Communications and Networking Conference (WCNC)*, pp. 1-6, Sydney, Australia, 2010.
- [9] C. Shen, Y. Zhu, S. Zhou and J. Jiang, "On the Performance of V-BLAST with Zero-forcing Successive Interference Cancellation Receiver," *Proc. of IEEE Global Telecommunications Conference (GLOBECOM'04)*, vol. 5, pp. 2818-2822, Dallas, TX, USA, 2004.
- [10] J. Han, X. Tao and O. Cui, "Lower Bound of BER in M-QAM MIMO System with Ordered ZF-SIC Receiver," *Proc. of the 69<sup>th</sup> IEEE Vehicular Technology Conference (VTC)*, pp. 1-5, Barcelona, Spain, 2009.

- [11] S. M. Maung, S. Hajime and S. Iwao, "Reduced Complexity Scheme for MIMO Receiver with Combined ZF-OSIC and ML Detection," Proc. of IEEE Symposium on Computers & Informatics (ISCI), pp. 92-96, Penang, Malaysia, 2012.
- [12] J. Wang, O. Y. Wen and S. Li, "Soft-output MMSE OSIC MIMO Detector with Reduced-complexity Approximations," Proc. of the 8<sup>th</sup> IEEE Workshop on Signal Processing Advances in Wireless Communications, pp. 1-5, Helsinki, Finland, 2007.
- [13] J. Wang and S. Li, "Soft-output MIMO MMSE OSIC Detector under MMSE Channel Estimation," Proc. of the 3<sup>rd</sup> IEEE International Conference on Communications and Networking in China, pp. 1117-1121, Hangzhou, China, 2008.
- [14] Y. Song, C. Liu and F. Lu, "The Optimal MMSE-based OSIC Detector for MIMO System," IEICE Transactions on Communications, vol. 99, no. 1, pp. 232-239, 2016.
- [15] H. Q. Ngo, E. G. Larsson and T. L. Marzetta, "Energy and Spectral Efficiency of Very Large Multiuser MIMO Systems," IEEE Transactions on Communications, vol. 61, no. 4, pp. 1436-1449, 2013.
- [16] Y. S. Cho, J. Kim, W. Y. Yang and C. G. Kang, MIMO-OFDM Wireless Communications with MATLAB, John Wiley & Sons, 2010.
- [17] P. N. Murthy and R. V. S. Satyanarayana, "A Comparison of Rayleigh and Rician Fading Channels under Frequency-selective Fading," IUP Journal of Electrical & Electronics Engineering, vol. 3, no. 4, 2010.
- [18] A. Moradi, H. Bakhshi and V. Najafpoor, "Pilot Placement for Time-varying MIMO OFDM Channels with Virtual Subcarriers," Communications and Network, vol. 3, no. 1, pp. 31-38, 2011.
- [19] I. Barhumi, G. Leus and M. Moonen, "Optimal Training Design for MIMO OFDM Systems in Mobile Wireless Channels", IEEE Transactions on Signal Processing, vol. 51, no. 6, pp. 1615-1624, 2003.
- [20] C. D. Cantrell, Modern Mathematical Methods for Physicists and Engineers, Cambridge University Press, 2000.
- [21] T.-L. Tung, K. Yao and R. E. Hudson, "Channel Estimation and Adaptive Power Allocation for Performance and Capacity Improvement of Multiple-antenna OFDM Systems," Proc. of the 3<sup>rd</sup> IEEE Workshop on Signal Processing Advances in Wireless Communications (SPAWC'01), pp. 82-85, Taiwan, China, 2001.
- [22] S. Yang and L. Hanzo, "Fifty Years of MIMO Detection: The Road to Large-scale MIMOs," IEEE Communications Surveys & Tutorials, vol. 17, no. 4, pp. 1941-1988, 2015.
- [23] P. Rajeev, A. Prabhat and L. Norsang, "Sphere Detection Technique: An Optimum Detection Scheme for MIMO System," International Journal of Computer Applications, vol. 100, no. 2, pp. 25-29, 2014.
- [24] G. J. Foschini, "Layered Space-time Architecture for Wireless Communication in a Fading Environment when Using Multi-element Antennas," Bell Labs Technical Journal, vol. 1, no. 2, pp. 41-59, 1996.
- [25] G. D. Golden, C. J. Foschini, R. A. Valenzuela and P. W. Wolniansky, "Detection Algorithm and Initial Laboratory Results Using V-BLAST Space-time Communication Architecture," Electronics Letters, vol. 35, no. 1, pp. 14-16, 1999.
- [26] P. W. Wolniansky, G. J. Foschini, G. D. Golden and R. A. Valenzuela, "V-BLAST: An Architecture for Realizing Very High Data Rates over the Rich-scattering Wireless Channel," Proc. of the IEEE Conference URSI International Symposium on Signals, Systems and Electronics (ISSSE 98), Cat. No.98EX167, pp. 295-300, Pisa, Italy, 1998.
- [27] A. Riadi, M. Boulouird and M. M. Hassani, "ZF/MMSE and OSIC Detectors for Uplink OFDM Massive MIMO systems," Proc. of the IEEE Jordan International Joint Conference on Electrical Engineering and Information Technology (JEEIT), pp. 767-772, 9-11 April 2019, Amman, Jordan, 2019.
- [28] A. Riadi, M. Boulouird and M. M. Hassani, "Least Squares Channel Estimation of an OFDM Massive MIMO System for 5G Wireless Communications," Proceedings of the 8<sup>th</sup> International Conference on Sciences of Electronics, Technologies of Information and Telecommunications (SETIT'18), vol. 2, pp. 440-450, Springer, Cham, 2018.
- [29] A. Riadi, M. Boulouird and M. M. Rabet Hassani, "Performance of Massive-MIMO OFDM System with M-QAM Modulation Based on LS Channel Estimation," Proc. of the 3<sup>rd</sup> International Conference on Advanced Systems and Emergent Technologies (IC ASET'2019), Hammamet, Tunisia, 19-22 March 2019.
- [30] A. Riadi, M. Boulouird and M. M. Hassani, "3-D Polarized Channel Modeling for Multipolarized UCA-

- Massive MIMO Systems in Uplink Transmission," Jordanian Journal of Computers and Information Technology (JJCIT), vol. 05, no. 03, pp. 231-243, December 2019.
- [31] J. Minango and A. C. Flores, "Low-complexity MMSE Detector Based on Refinement Jacobi Method for Massive MIMO Uplink," Physical Communication, vol. 26, pp. 128-133, 2018.
- [32] S. Wang, Y. Li, M. Zhao and J. Wang, "Energy Efficient and Low-complexity Uplink Transceiver for Massive Spatial Modulation MIMO," IEEE Transactions on Vehicular Technology, vol. 64, no. 10, pp. 4617-4632, 2014.
- [33] S. Wu, L. Kuang, Z. Ni, J. Lu, D. Huang and Q. Guo, "Low-complexity Iterative Detection for Large-scale Multiuser MIMO-OFDM Systems Using Approximate Message Passing," IEEE Journal of Selected Topics in Signal Processing, vol. 8, no. 5, pp 902-915, October 2014.
- [34] M. Aldababseh and A. Jamoos, "Estimation of FBMC/OQAM Fading Channels Using Dual Kalman Filters," The Scientific World Journal, vol. 2014, Article ID 586403, 2014.
- [35] O. E. Ijiga, O. O. Ogundile, A. D. Familua and D. J. J. Versfeld, "Review of Channel Estimation for Candidate Waveforms of Next-generation Networks," MDPI Electronics, vol. 8, no. 9, Article no. 956, 2019.
- [36] K. E. Baddour and N. C. Beaulieu, "Autoregressive Modeling for Fading Channel Simulation," IEEE Transactions on Wireless Communications, vol. 4, no. 4, pp. 1650-1662, July 2005.

### ملخص البحث:

في هذه الورقة، يتم البحث في تخمين القنوات بطريقة المربعات الصغرى (LSCE) في الأنظمة الضخمة متعددة المداخل متعددة المخارج القائمة على النغمات الإرشادية. وقد تم أخذ الإرسال المعتمد على الربط العلوي (UL) بعين الاعتبار، بحيث جرى اقتراح طريقة لتخمين القنوات عبر تكوين معادلة في هيئة مصفوفة تشتمل على جميع متغيرات القنوات غير المعروفة في متجه واحد وتخمينه باستخدام طريقة المربعات الصغرى. وقد تم حساب متوسط الخطأ التربيعي (MSE) لتخمين القنوات بطريقة المربعات الصغرى (LSCE).

وقد جرى تقييم الخُفوت المستوي والخُفوت المعتمد على الإنتقائية الترددية لرمز واحد ولرموز متعددة من رموز الإرسال المضاعف المتعامد القائم على التقسيم الترددي (OFDM) فيما يتعلق بمتوسط الخطأ التربيعي (MSE). كما تم استقصاء المتطلب الخاص بتتابع العلامات الإرشادية في كل من الخُفوت المستوي والخُفوت المعتمد على الإنتقائية الترددية. الى جانب ذلك، اتضح أنّ عدد العلامات الإرشادية يؤدي الى وضع تسويات مرغوبة بين هوائيّ المحطة الأساسية وتفرعات القنوات. وقد جرى اعتبار خُفوت القنوات المعروف بخُفوت قنوات رايلي (Rayleigh) وخُفوت قنوات ريسان (Rician) لتقييم أداء النظام باختلاف عدد تفرعات كل قناة من القنوات. وتم تقييم الأداء بناءً على قيم معدل الخطأ في البتات (BER). علاوة على ذلك، من أجل تحسين أداء الكواشف الخطية، تم استخدام كواشف غير خطية. وتبين أن متطلب تتابع العلامات الإرشادية وزيادة تنوع الاستقبال تؤدي الى تقليل قيمة معدل الخطأ (BER).

